AIAA Guidance, Navigation, and Control Conference
08 - 11 August 2011, Portland, Oregon

AIAA 2011-6662

Real-time Wind Profile Estimation using Airborne Sensors

A.C. in 't Veld[*], P.M.A. de Jong[†], M.M. van Paassen[‡], M. Mulder[§]
Delft University of Technology, P.O. Box 5058, 2600 GB Delft, The Netherlands

Wind is one of the major contributors to uncertainty in continuous descent approach operations. Especially when aircraft that are flying low or idle thrust approaches are issued a required time of arrival over the runway threshold, as is foreseen in some of the future ATC scenarios, the on-board availability of both dependable and accurate wind estimates becomes a necessity. This paper presents a method for real-time estimation of a wind profile in the terminal maneuvering area, based on data transmissions of nearby aircraft that produces real-time wind profile estimates in a form that is usable for accurate trajectory estimation. The wind estimation algorithm is designed to process data that is of the form currently used in the Aircraft Meteorological Data Relay (AMDAR)-program. The algorithm combines a stochastic estimation based on this data and a traditional logarithmic estimator in order to be able to produce a valid estimation even when there are no data available from other aircraft.

I. Introduction

Various research into advanced Continuous Descent Approaches procedures such as Tailored Arrivals,[1,2] the LAX descent procedures and the time-based Three-Degree Decelerating Approach[3–5] have shown that accurate trajectory prediction is only possible with a sufficiently accurate wind model. Such a wind model needs to have a fine resolution and high update frequency to be able to cater for the fast changing wind profile as experienced by aircraft flying an approach. Different approaches have turned to different solutions, ranging from a simple profile based on the wind measured on-board the aircraft and the wind report at the runway,[1] to up-linking entire high resolution wind grids from the National Oceanic and Atmospheric Administration (NOAA).[2]

This research proposes a relatively easy approach of implementing a wind profile estimator capable of producing real-time wind profiles with sufficiently high resolution that they are usable for accurate trajectory prediction on-board an aircraft flying an advanced approach procedure. The idea is to leverage on the fact that in th near future aircraft will be equipped with data-link capability such as ADS-B which allows aircraft to gather state information from nearby aircraft. In fact the aircraft in the Terminal Maneuvering Area (TMA) can be seen as a set of airborne weather sensors providing among other data current wind speed and direction at their location.

The idea of using aircraft data to improve meteorological data is not new. The Aircraft Meteorological Data Relay program (AMDAR) was first proposed by the World Meteorology Organization in the 1970s and has been using aircraft data to improve their weather models since the late 1990s.

Because of the high degree of variability and hence unpredictability of wind profiles near the ground, a wind estimation algorithm has been developed[3,4] that uses AMDAR, providing wind speed measurement data and other meteorological data. In this research, the algorithm has been made applicable to the three-dimensional situation of the TMA.

The paper starts with an introduction into a physical wind model and continues in Section III with an overview of the wind estimator algorithm. The performance of the algorithm is reviewed in Section IV. Finally, a conclusion is drawn in Section V.

[*]Researcher, Control and Simulation Division, Faculty of Aerospace Engineering, Delft University of Technology. Kluyverweg 1, 2629 HS Delft, The Netherlands. AIAA Member. E-mail: a.c.intveld@tudelft.nl
[†]PhD-Student, Control and Simulation Division, Faculty of Aerospace Engineering, Delft University of Technology. Kluyverweg 1, 2629 HS Delft, The Netherlands. AIAA Student Member. E-mail: p.m.a.dejong@tudelft.nl
[‡]Associate Professor, Control & Simulation Division, AIAA Member
[§]Professor, Control & Simulation Division, AIAA Senior Member

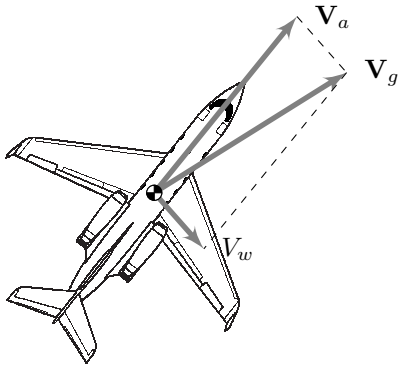

Figure 1. Calculation of the Wind Speed Vector

I.A. AMDAR Characteristics

Modern commercial aircraft are equipped with meteorological sensors and associated sophisticated data acquisition and processing systems. These provide input in real time to the aircraft flight management, control and navigation systems and other on-board systems.[6] Aircraft participating in the AMDAR project automatically relay (a selection of) these data to the ground receivers. This is usually done through the Aircraft Communication Addressing and Reporting System (ACARS) system, or a satellite based equivalent. According to AMDAR specifications, the elements to be reported in a single observation are position (latitude and longitude) and altitude, time, temperature, wind direction and speed, turbulence, humidity and icing, phase of flight, some aircraft state variables such as roll and pitch angles, and an aircraft identifier.

The wind speed is calculated by resolving the two speed vectors V_a, the measured true airspeed, and the groundspeed V_g, which is calculated within the FMS (typically based on IRU and GPS data), see Fig. 1. The accuracy of both speed vectors (in magnitude and direction) is about 2-3 m/s and 1°.[6,7]

Obviously, the meteorological reports are spatially concentrated around the busiest routes at cruise altitudes and in the TMAs around the major airport hubs. This will lead to a loss of accuracy in the wind estimation at less crowded airports or during slow traffic hours. This is not expected to cause any problems since in these situations the demanded runway capacity is usually substantially less than the maximum available capacity and less accuracy is acceptable.

As of yet, no broadcasting standard has been defined. Data may be transmitted through VHF, ADS-B, Mode S or a satellite communication system. The source and broadcasting method of the available data are not of particular concern to this research.

I.B. The Wind Estimation Algorithm

The obtained wind observations are first grouped together into altitude intervals of for instance 500 ft. Next, the noise in the data is filtered out. The smoothed data is then used to get a wind estimation for every altitude interval over a short-term time interval. These estimated wind speeds and directions are then combined to form the estimated wind profile. The complete process is repeated when new observation data has been collected. Every step of this iteration process will be explained in more detail in the next sections.

A Kalman filter has been selected for the wind data smoothing task.[8,9] The purpose of the filter is to extract the noise components of the measured wind data and to assign smaller weights to measurements that were taken farther in time or are taken at a larger distance from the reference trajectory. Finally, the estimated wind profile (speed or direction) is created by simple linear interpolation through the estimated wind speeds.

The algorithm is run separately for wind speed and wind direction to avoid non-linearities. In both cases, the state vectors would be equal in size but the noise matrices contain different values to account for the difference in accuracy of the respective sensors.

The strength of this wind estimation algorithm is its flexibility.[3,4] It provides an accurate profile based on a statistical model when sufficient data is present. This has the added benefit that the accuracy increases when the traffic density increases, for example when accurate trajectory prediction is most important.

Aircraft without ADS-B In capabilities or insufficient FMS computational power could receive an estimated profile generates by a ground station that receives soundings from aircraft in its vicinity. The

update rate and accuracy will be lower but at least wind data will be available to these aircraft.

II. Physical Wind Model

Wind is one of the primary atmospheric factors affecting airplane performance. It is the movement of air relative to the Earth. Wind can be quantitatively described with its velocity and its direction. The wind direction is defined as the direction from which the wind originates. Wind direction is defined in the Earth reference frame F_E. The movement of air is mainly the result of three major mechanisms being air pressure gradients, the influence of the rotation of the Earth and the surface friction forces.[10]

1. The air pressure gradients are caused by the uneven distribution of solar heat over the Earth on a large scale (Equator to Polar region) and on a minor scale (local natural and artificial heat sources and sinks like lakes, cities, etc.).

2. The rotation of the Earth induces a force that acts on moving air. This force is called the Coriolis force.

3. The surface friction force arises from the relative motion of the air with respect to the ground. The influence of the friction force is naturally larger closer to the Earth's surface. Its magnitude is mainly dependent on the degree of roughness of the terrain.

Hence, three mechanisms are able to influence the movement of air. Two of them, the rotation and the solar heating of Earth, define the always present gradient force G and Coriolis force C. The friction force W on the other hand depends on the distance to the surface and can be neglected at high altitudes. So two alternative situations arise, presented in Fig. 2.[10,11] Fig. 2(a) shows a non-friction situation which is valid at large distance from the Earth surface. The Coriolis force C has to balance the gradient force G to ensure the equilibrium. As a result the wind vector U is parallel to the isobars since the Coriolis force is always perpendicular to the wind vector. The wind velocity in this "frictionless" part of the atmosphere ("free" atmosphere) is usually called the *geostrophic wind* U_g.
Fig. 2(b) describes the lower part of the atmosphere where surface friction is no longer negligible. A surface friction force W arises along the wind vector U in opposite direction. The gradient force G remains fixed. As a result, the gradient force needs to be balanced by the resultant of the Coriolis force and the friction force. Therefore the wind direction changes over an angle and the magnitude of the wind decreases. The wind velocity decreases gradually from its geostrophic value to zero at the ground. The deviation of the wind direction with respect to the geostrophic wind (β) becomes larger when the friction force increases, so closer to the ground. In the Northern hemisphere the wind vector rotates counter clock-wise with decreasing altitude. This layer of the atmosphere where surface friction occurs is called the Planetary Boundary Layer (PBL). Its top is typically between 200 m and 2,000 m above the surface.[12]

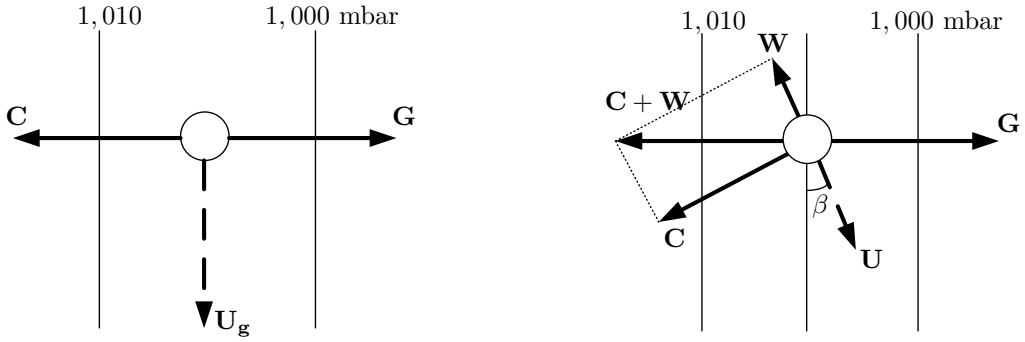

(a) Geostrophic wind, no friction.

(b) Change of wind due to friction.

Figure 2. Influence of pressure gradient force (G), Coriolis force (C) and friction force (W) on movement of air in Northern hemisphere[10]

The above describes the general mechanism of wind generation on a large scale. But wind is also influenced locally by specific surface obstacles such as trees, buildings, etc. and by local differences in temperature. These distortions can be of great influence on the local wind profile. For this analysis the effect of local obstacles is less important, since they influence the wind profile only very close to the ground (< 1,000 ft). For the accurate execution of continuous descent approaches it is acceptable to use the general surface roughness classification. The local temperature differences define the local stability

of the atmosphere. The atmospheric stability is of more interest since it influences the wind profile over the whole PBL. This will be elaborated further in the next section.

II.A. The Atmospheric Stability

The atmospheric stability is one of the mechanisms that influences the local wind profile of the planetary boundary layer (PBL). The gradient of the wind velocity with the altitude depends on the amount of horizontal motion that is exchanged vertically.[13] The momentary temperature profile determines this stability, one of the major factors is the rate of change of air temperature with altitude.[14] Due to time evolution in terms of changing vertical thermal build-up, the boundary layer is a rather complicated object. The PBL has three broad types of structure with typical characterizing conditions,[13]

1. Unstable/convective boundary layers; light winds and a high surface heat flux
2. Neutral boundary layers; high winds and/or small surface heat flux
3. Stable boundary layers; light winds and a negative surface heat flux (most during night time)

The strong vertical heat exchange in an unstable atmosphere causes the horizontal wind speed to be maximally exchanged downwards.[10] As a result, the mean wind has a sharp increase near the surface. But throughout most of the boundary layer the mean flow is fairly uniform.[13] The stable boundary layer is the most variable of the three kinds of layers and is usually in a continuous state of evolution. This usually occurs between the hours of sunset and sunrise when the surface is cooling or when warm air moves over a cool surface. In these conditions there is very little vertical exchange of wind. This can lead to light winds near the surface and strong winds up in the atmosphere. Typical wind profiles for a stable atmosphere are illustrated by the solid line in Fig. 3. The stable boundary layer is more responsive to Coriolis accelerations. This leads to the direction of the wind changing over the depth of the layer by 25-40°.[13]

In neutral boundary layers the wind profile does not depend on the vertical heat exchange but only on the surface roughness. The atmosphere has a neutral stability when clouds are present or in case strong winds occur. Extended cloud cover reduces the warming or cooling of the Earth's surface leading to little vertical heat exchange. With strong winds the vertical exchange of winds can be considered purely mechanical, the thermal effects are negligible.[10,11] The wind profile of a neutral boundary layer lies between the two extremes of a stable and unstable atmospheric condition.

Several wind measurements presented in the work of Wieringa (1987)[12] indicate that the difference in wind velocity of stable/unstable versus neutral atmospheric conditions remains relatively small. For instance, the daily change of mean wind velocity over 18 days of clear sky at an altitude of 124 m varied between 9 m/s (night) and 5 m/s (day).[12] Other wind data, presented in Fig. 3, show a maximum difference of 4 m/s between the stable (solid line) and unstable wind profile (dashed line) at 350 m above the ground for 81 days of clear skies. During 129 clouded days the mean maximum difference was only 1 m/s. The wind profile of a neutral boundary layer lies between the two extremes of a stable and unstable atmospheric condition. So in the examples above, the maximum deviation of the wind velocity with respect to a neutral wind profile will be smaller than 4 m/s. The measured differences will probably increase a little for geostrophic winds that are somewhat stronger than 8 m/s. Nevertheless the deviations are expected to remain of the same order as the atmospheric boundary layer tends to get more neutrally stable with increasing wind.

For an efficient execution of a continuous descent approach a good estimation of the wind profile is necessary. The accuracy of the estimation becomes more critical when stronger winds occur. For these conditions a wind profile for a neutral boundary layer is applicable. In case of light winds and clear skies, the wind profile changes continuously due to the daily evolution of the stability in the PBL. The daily wind pattern changes from an unstable atmosphere during the day to a stable boundary layer during the night. The amplitude of the daily evolution varies on his turn with the seasons and depends on the climate. It can be concluded that these atmospheric evolutions are very complex and have much variety, so the modeling of the wind could be simplified a lot by assuming neutral stability at all times.

These observations indicate that the neutrally stable wind profile could be taken as an approximation to cover all situations of the planetary boundary layer.

Given the above considerations, it can be concluded that it is justified to assume a neutral atmospheric boundary layer.

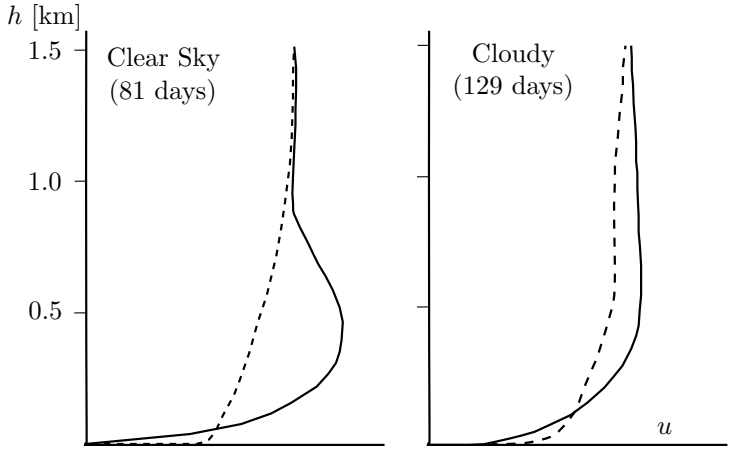

Figure 3. Mean wind profile for clear and clouded skies at Warszawa 1960; solid line = 0h00, dashed line = 12h00.[12]

II.B. The Mathematical Wind Model in Neutrally Stable Atmosphere

Different models have been used in literature to describe the wind profile in a neutrally stable planetary boundary layer. This section discusses these methods and defines which mathematical model will be used in this research. Before continuing it is important to know that the planetary boundary layer can be subdivided in two layers,[12]

- The lowest 20% of the PBL is the *surface layer*, usually with the top between 60-100 m. Here some simplifications may be applied that are not allowed for the whole PBL, for instance neglecting the Coriolis force.
- The other 80% of the PBL is the so-called "Ekman layer" where the profile is influenced by both friction and Coriolis force.

Since aircraft flying an approach generally need to be configured for landing and maintaining a stabilized airspeed by the time they reach 1,000 ft above the ground, only the wind profile in the "Ekman layer" is of interest.

Hewitt and Jackson give the following mathematical description of the wind profile in the neutral boundary layer.[13] Over the lowest 100 m the profile is logarithmic and depends on roughness length z_0. In the upper part of the boundary layer, the profile depends on (z/h) and the power-law profile is a useful approximation. There is a systematic turning of the wind with height due to the Coriolis acceleration, ranging from about 5° to 20°. The direction and magnitude of this turning is quite sensitive to changes in surface roughness and upper-layer conditions. Furthermore the strength of the Coriolis-force is dependent on the latitude.

Wind profiles are traditionally estimated with the *power-law*,[12]

$$V = V_0 \left(\frac{h}{h_0} \right)^p \tag{1}$$

where the windspeed V at altitude h is dependent on the windspeed V_0 at a reference height h_0. The exponent p is empirically derived constant, which for neutrally stable atmosphere is approximately $\frac{1}{7}$.[15] When the reference point (h_0, V_0) is chosen to fit the actual situation best, this equation only yields a very general approximation of the wind profile in the PBL. Especially since the PBL is characterized by the interaction between the free stream wind at higher altitudes and the disturbing forces of friction caused by the Earth's roughness, this approximation can differ significantly from the true wind profile. In order to derive a generally useful model that is not dependent on local surface roughness or the local latitude, the power-law is used as a baseline for the first approximation of the wind profile and could also be used to fill the gaps when measurement data is sparse. Subsequent estimates of the wind-profile are updated using available data from other aircraft as will be explained in the next section.

III. Airborne Wind Estimation Algorithm

The spatial and temporal variations of the wind affect the performance of the aircraft along the approach trajectory in the Earth-fixed reference frame. Accurate knowledge of the wind profile in the

TMA is therefore required for an accurate own trajectory prediction and time-to-fly estimates. The wind profile is modeled using a statistical model. The advantage of such a model is that it does not rely on the physical processes that govern wind behavior but instead uses observations to estimate any profile shape. On the other hand, a logarithmic profile estimate based on the power-law (Eq. (1)) is able to provide at least an initial estimate when data are insufficiently available. This way the algorithm combines the best of both worlds. Moreover, when data is sparse, a logarithmic profile, based on the latest profile estimate could serve as an intermediate 'estimate'. However, the research in this paper only uses a logarithmic profile when the algorithm is initiated and no wind data is available at all.

In the near future various data-link scenarios are envisaged; for instance in the SESAR and NextGen programs.[16–18] As the details of the proposed data-link systems such as ADS-B are not yet fully developed, the current algorithm is based on the format of the AMDAR data. With the transmission of AMDAR-like meteorological data to nearby aircraft a wealth of meteorological information will become available for processing either board the aircraft or in ground-based system. Currently, ACARS is the communication system most widely used by aircraft participating in the AMDAR program.

The wind estimation model is driven by historical AMDAR data, which consist of meteorological observations such as wind speed and direction as well as position coordinates. They are broadcast through a communication system (e.g., ACARS, Mode S, or ADS-B In/Out) to in-trail aircraft which then store the historical data in the Flight Management System (FMS) database. The data are processed to make estimates of the current and future wind profile by filtering the historical data. The algorithm is designed with a high-traffic scenario in mind but when the number of historical AMDAR observations available is scarce (e.g., between arrival and departure peaks), a wind profile can still be constructed using the available data, without making predictions. When an estimation is available, an Auto-Regressive Time Series could be generated to generate a wind profile prediction in time. However, research showed that this prediction is often less accurate then a simple Persistence Filter[5] which is used in the research described in this paper.

The algorithm consists of several steps. First, AMDAR data of preceding or nearby aircraft, each tagged with a corresponding time and altitude interval, is collected and stored in the FMS. Second, per altitude interval, the historical AMDAR data are filtered using a Kalman filter to remove measurement noise from the observations. Subsequently, the wind profile is constructed by connecting the results per altitude interval by linear interpolation.

The estimation algorithm uses incoming wind observation data from other aircraft within a certain range (for instance the TMA). The algorithm can be run either in the air, where data are processed on-board in the FMC, or on the ground; in this case the wind profile estimation could be up-linked to the aircraft.

The spatial coverage of AMDAR data makes it suitable for the wind estimation algorithm as the observations are made near and often on the same approach track. Temporal coverage of AMDAR data is highly variable due to peaks and lows in air traffic density. Fig. 4 shows a schematic of spatial and temporal coverage of AMDAR data. Obviously, wind estimation improves in high density traffic environments where aircraft spacing is critical to maintain high runway capacity.

The accuracy of AMDAR data depends on instrument measurement errors. Sources of error include calibration error, short-term random instrument error, calibration drift and static source error, which are corrected by the Air Data Computer. Typical uncertainty of AMDAR data is in the range between 2-3 m/s and $\approx 1°$.[6,7] System cross checks, gross error limits and outlier rejection are various methods used by the onboard quality monitoring system to eliminate bad data. Note that these measurement and quality monitoring systems may differ per aircraft type, which subsequently may affect the accuracy of the AMDAR data.

Wind profile estimation in three dimensions is possible. Using all available measurements throughout the TMA and tagging them with position information, the algorithm can calculate the profile estimate based not only on height, but also on horizontal position. Running the algorithm for wind speed and direction separately, yields a 2-dimensional estimation along any 3-dimensional path through the TMA.

III.A. Kalman Filtering and Algorithm Design

This section assumes that the algorithm runs on an onboard FMS but the derivations are similar in case a ground station constructs wind profiles estimates. The following steps are taken in the construction of the wind profile estimation algorithm.

- Determine the nominal flight track. This track is the intended approach route under normal circumstances. Along this track, the wind profile will be estimated. The altitude resolution of the state vector is chose arbitrarily, but in this case set to 500 ft. It is noted that the accuracy of

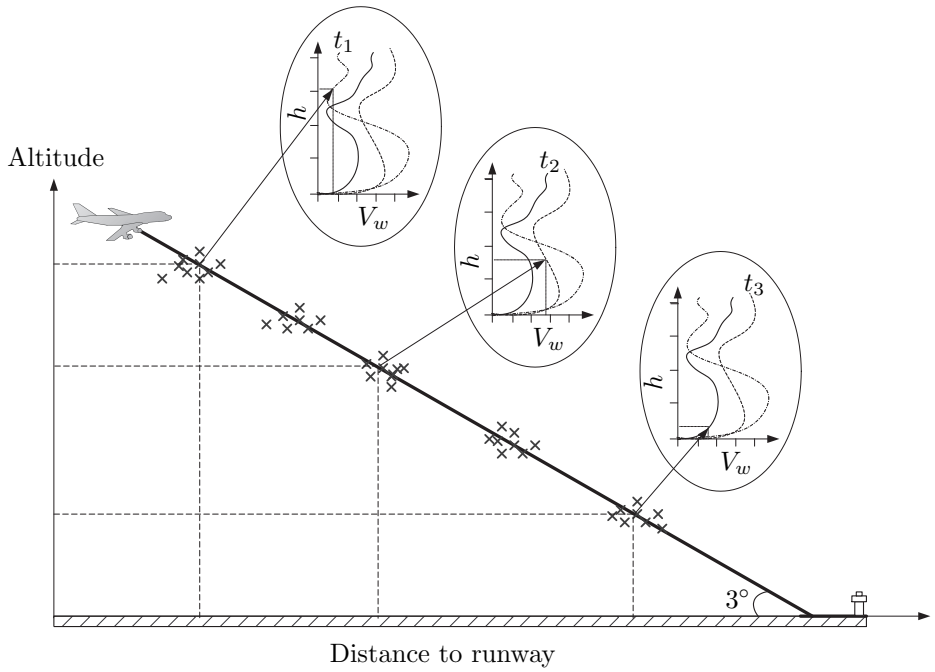

Figure 4. Time-dependent wind profile estimation. Spatially distributed AMDAR observations are represented by crosses. Each set of AMDAR observations is associated with an altitude, a longitude and a latitude.

the estimation depends on the accuracy, the amount and the spatial and temporal spread of the incoming data, and not on the resolution of the state vector.

- Generate an initial estimate when the first wind measurements come in. These might be either a nominal wind speed at certain altitude provided by ATS, or the first incoming data from ADS-B soundings from other aircraft. Based on these first measurements, a standard logarithmic wind profile is constructed according to Eq. (1). Hence, this logarithmic profile becomes the initial state estimate, which will be updated whenever new data comes available.
- After this the filter is updated every second (1 Hz).

The general Kalman state equation and measurement equation are given by respectively,

$$\begin{aligned} x(k) &= A(k|k-1)x(k-1) + w(k-1) \\ y(k) &= C(k)x(k) + v(k) \end{aligned} \tag{2}$$

with,

$$\begin{aligned} Q &= \mathbb{E}\left\{ww^T\right\} \\ R &= \mathbb{E}\left\{vv^T\right\} \end{aligned} \tag{3}$$

In Eq. (2) $x(k)$ is the wind *state*[a] at time k, $A(k|k-1)$ is the transition matrix and $w(k-1)$ is the process noise. In the measurement equation, $y(k)$ is the measured wind speed at time t, $C(k)$ is the measurement matrix and $v(k)$ the measurement noise. Since no system dynamics are used in the model, the transition matrix $A(k|k-1) = I(n \times n)$, where n is the number of states to be estimated (depending on the altitude resolution). When the measurements exactly match the altitude resolution of the state vector, the measurement matrix $C(k) = I(m \times n)$.

The elements of the Kalman filter are constructed through steps 1 - 6 t time instant k as follows,

1. The state vector $\hat{x}$ is an $n \times 1$ vector, where n is the number of altitudes, depending on the chosen resolution (in this case 500 ft, depicted as Flight Levels). The state estimate, $\hat{x}(k|k-1)$ is,

$$\hat{x}(k|k-1) = \begin{pmatrix} v_w^0 & v_w^{05} & v_w^{10} & v_w^{15} & \dots & v_w^{100} \end{pmatrix}^T \tag{4}$$

[a]In this paper, we only treat the estimation of wind speed but the same principles apply to wind direction.

2. When an observation comes in, the wind speed or direction are stored, along with the altitude at which the observation was recorded (for example 1700 ft, FL 17),

$$y(k) = \begin{pmatrix} v_w^{17} \end{pmatrix} \tag{5}$$

3. In the next step, the weighing matrix $C(m \times n)$ is set up, where m indicates the amount of incoming observations. The C matrix determines which elements of the state vector can be updated when a measurement comes in. In this case, it is the two points that are closest to the altitude of the measurement. The weights in the matrix are determined based on the altitude difference between the states of interest and the measurement.

$$C(k) = \begin{pmatrix} c_1^0 & c_1^{05} & c_1^{10} & c_1^{15} & c_1^{20} & \dots & c_1^{100} \\ c_2^0 & c_2^{05} & c_2^{10} & c_2^{15} & c_2^{20} & \dots & c_2^{100} \\ \vdots & \vdots & \vdots & \vdots & \vdots & \ddots & \vdots \\ c_m^0 & c_m^{05} & c_m^{10} & c_m^{15} & c_m^{20} & \dots & c_m^{100} \end{pmatrix} \tag{6}$$

In this example, with an observation recorded at FL 17 (so between FL 15 and FL 20), the C matrix is filled as,

$$C(k) = \begin{pmatrix} 0 & 0 & 0 & 0.6 & 0.4 & \dots & 0 \end{pmatrix} \tag{7}$$

4. With this C matrix, the current estimate for the altitude of the observation can be calculated, and its value can be compared to the measured value to determine the innovation $e(m \times 1)$,

$$\hat{y}(k|k-1) = C(k)\hat{x}(k|k-1) \tag{8}$$

$$e(k) = y(k) - \hat{y}(k|k-1) \tag{9}$$

This way, an incoming measurement only influences the states in its (vertical) vicinity. This is also shown in Fig. 5, where the encircled elements of the state vector are the updated values.

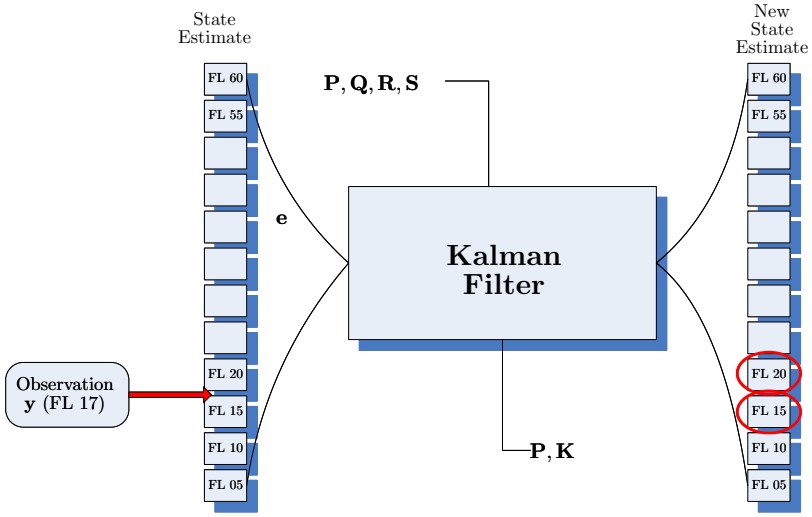

Figure 5. State estimate update schematic. The encircled elements of the state vector around the observation altitude are updated.

5. This innovation is to be multiplied with the Kalman gain to obtain a new state estimate. The Kalman gain is based on the relative magnitudes of the uncertainties in the current estimate and the new measurement. The measurement noise covariance matrix $R(m \times m)$ depends on the shortest distance between the location of the measurement and the own track d,

$$R(k) = \begin{pmatrix} R_1^{alt} + \alpha d(k) & 0 & 0 & \dots & 0 \\ 0 & R_2^{alt} + \alpha d(k) & 0 & \dots & 0 \\ \vdots & \vdots & \vdots & \ddots & \vdots \\ 0 & 0 & 0 & \dots & R_m^{alt} + \alpha d(k) \end{pmatrix} \tag{10}$$

where α is assigned a value of 0.5 (if d is in nautical miles), which is not investigated or tested. So for the single measurement at 1700 ft, the R matrix is,

$$R(k) = \begin{pmatrix} R_1^{17} + 0.5 \cdot d(k) \end{pmatrix} \tag{11}$$

In the next sub-step, the covariance of the estimate is projected ahead using the process noise covariance matrix ($Q(n \times n)$),

$$P(k|k-1) = P(k-1|k-1) + Q(k-1) \tag{12}$$

With this projection, the covariance of the innovation step can be represented by the matrix $S(m \times m)$,

$$S(k) = C(k)P(k|k-1)C(k)^T + R(k) \tag{13}$$

where $P(n \times n)$ is the prediction error covariance matrix. These matrices together determine the Kalman gain $K(n \times m)$,

$$K(k) = P(k|k-1)C(k)^T \left(C(k)P(k|k-1)C(k)^T + R(k)\right)^{-1} \tag{14}$$

A high [low] uncertainty in the current estimate (high [low] P) and much [little] confidence in the accuracy of the measurement (low [high] S) yields a high [low] value of the Kalman gain, which in turn assigns a large [small] weight to the incoming observation in updating the state estimate through the innovation,

$$\hat{x}(k|k) = \hat{x}(k|k-1) + K(k)e(k) \tag{15}$$

6. In the final step, the prediction error covariance matrix P is updated, according to,

$$P(k|k) = (I - K(k)C(k))\, P(k|k-1) \tag{16}$$

It can be seen that when no new observation data is available, there will be no innovation, and the loop is reduced to updating the prediction error covariance P. In this way, the uncertainty about an estimate increases when time goes by without new incoming measurements. A schematic of this loop is given in Fig. 6.

Fig. 7 shows that the initial estimate (solid line), based on the single first incoming measurement, equals the logarithmic profile. For this estimate, the initial prediction error matrix P is set high, which will yield a high Kalman gain, giving a high weight to the first set of observed data. The starred dots represent the actual incoming measurements, and the dashed line is the new wind profile estimate. Seven minutes later new data broadcasts have come in. Based on these measurements, the previous estimate (solid line in Fig. 8) is updated to become the solid line in Fig. 8, and so forth.

The influence of the measurement noise covariance R is shown in Fig. 8(b). This plot is based on the same data as Fig. 8(a), but used a higher value of R, simulating the effect of a distant measurement. Since this higher value indicates 'noisier' measurements, their influence on the update of the wind profile decreases. Clearly, when the uncertainty in the measurements is low, the estimate follows the data much more closely.

III.B. Wind profile construction

The output of the algorithm is a set of estimations per 500 ft altitude interval along the planned arrival trajectory, which represent the evolution of the wind speed or direction along the time axis, starting from the present time of the aircraft until the time t minutes ahead at the end of the approach procedure. For each estimation step, the wind profile is constructed by connecting the estimations per altitude interval by linear interpolation.

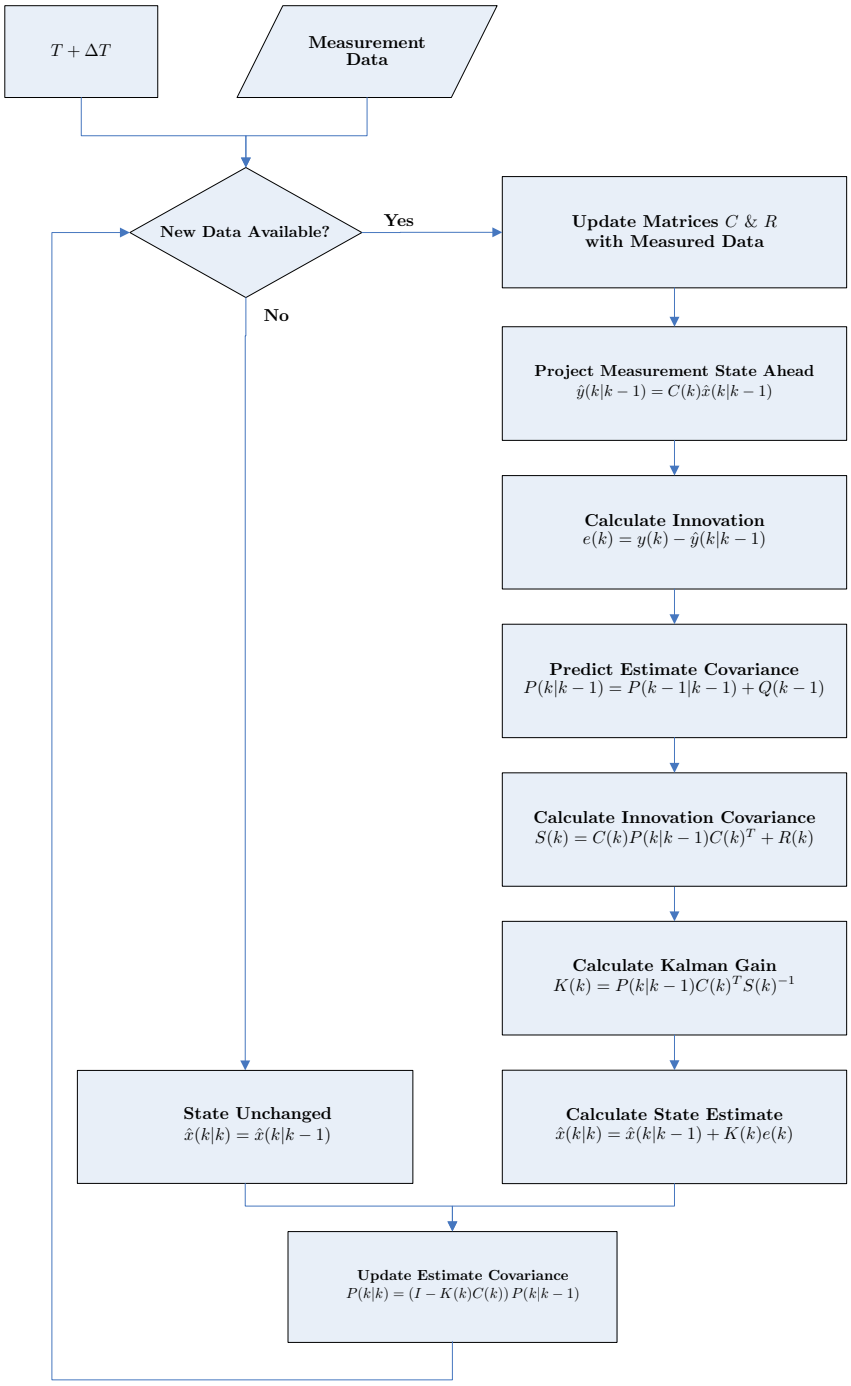

Figure 6. Kalman filter schematic.

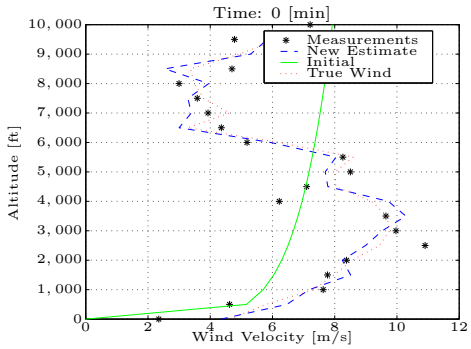

Figure 7. Wind speed update process, T = 0 minutes.

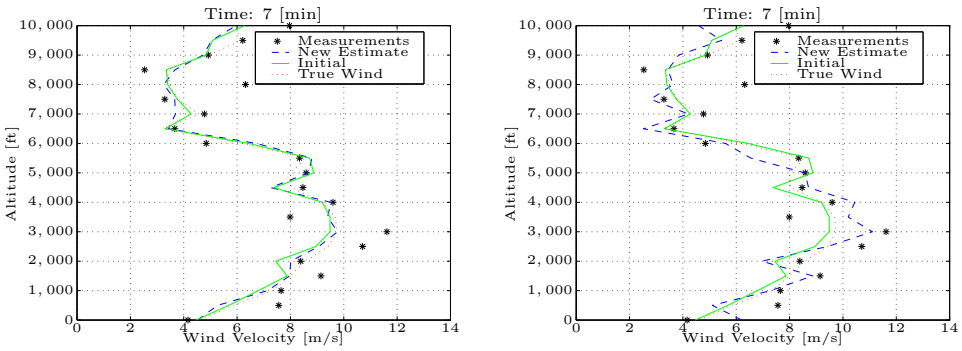

(a) low R. (b) high R.

Figure 8. Wind speed update process, T = 7 minutes.

IV. Wind Estimation Performance Evaluation

The functioning of the wind estimator in an off-line simulation is visualized in Fig. 10. For this specific simulation, measurement data from soundings at Chicago O'Hare (see Fig. 9) from nine consecutive incoming or outgoing aircraft (in multiple bearings) have been used. As these aircraft fly through the TMA, measuring and broadcasting (a.o.) wind speeds, the filter is updated every time step when new data is received. The observations are combined by a ground station and preprocessed to fit the state vector of 500 ft intervals. So every time an aircraft passes along its data, a new estimate is constructed by the ground station. Fig. 10 shows the development of the wind profile with every new time interval.

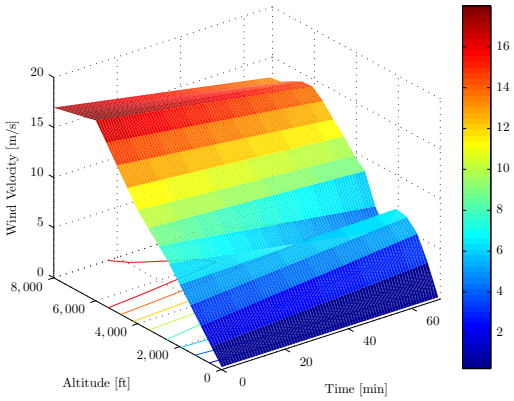

Figure 9. Time-dependent wind profile at Chicago O'Hare on the 7$^{\text{th}}$ of January 2005.

Since the filter uses the relative distance between the location of the measurement and the own trajectory (or position in case of a ground based station) to adjust the measurement error covariance matrix R, an arbitrary 3-dimensional approach path has been set up for the own aircraft. An example of such a path is shown in Fig. 11.

IV.A. Check on relevant parameters

The most important parameters calculated in the Kalman filter (as described in Section III.A) are the innovation step (the difference between the 'projection ahead' at a certain point of interest and the actual value measured at that same point) and the Kalman gain. For a single aircraft passing along the altitudes of interest the response of these quantities is shown in Fig. 12(a). Shown in this figure are incoming wind profiles from a ground station, running at 1 Hz and observations from a single aircraft descending through the altitudes of interest of our own aircraft which is flying at 4,500 ft. The interval of interest is thus 4,000 - 5,000 ft. Seen in Fig. 12(a) is that after approximately 25 minutes the descending aircraft reaches the relevant altitude range, and its broadcasts are used to update the wind profile estimate. From this moment on, every innovation step is assigned a weight (the Kalman gain, depicted with the dot-dashed line), to determine the new estimate for this altitude.

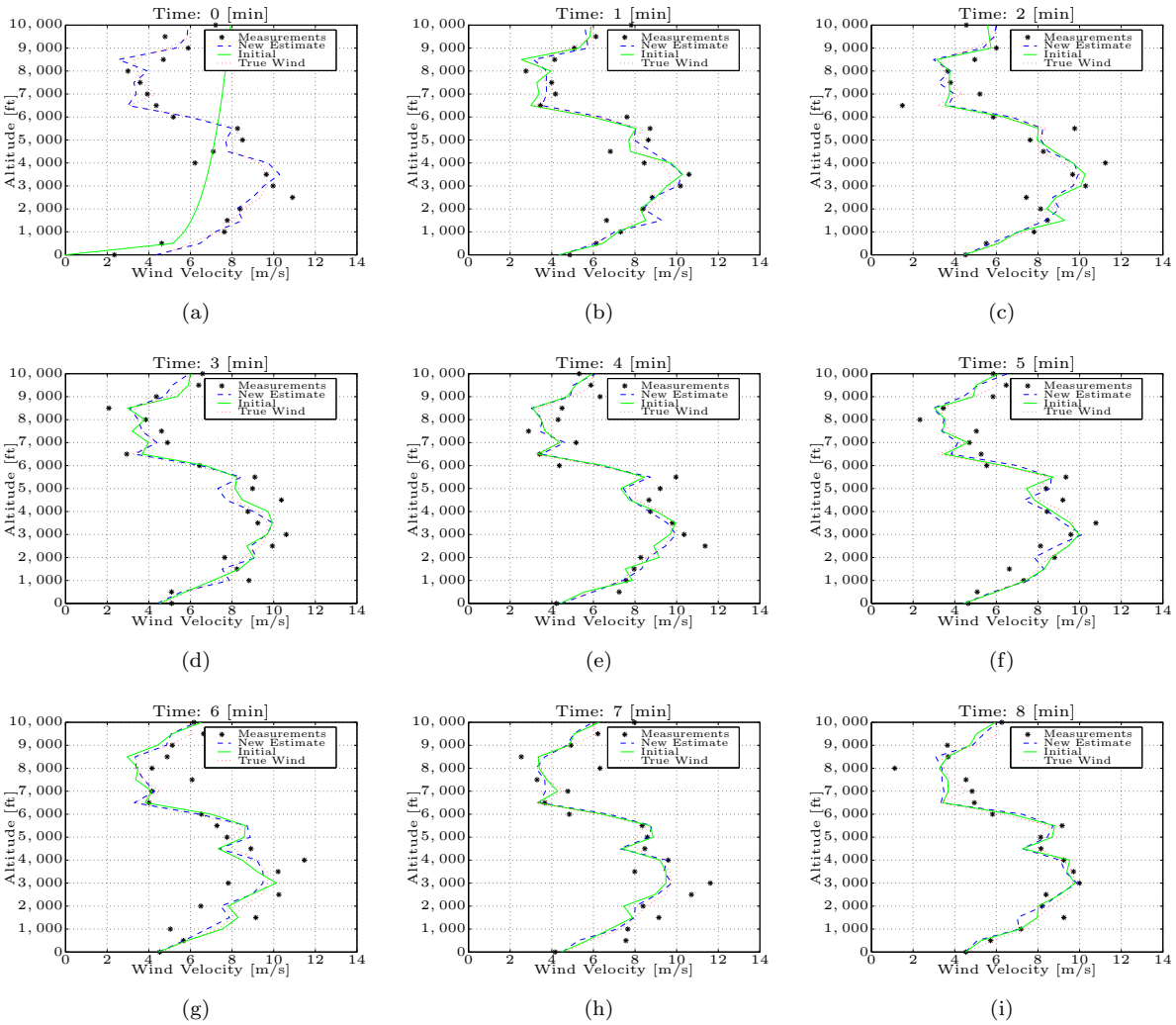

Figure 10. Influence of new data from subsequent incoming aircraft on the wind profile estimation. Each new estimate becomes the 'initial estimate' in the next subfigure.

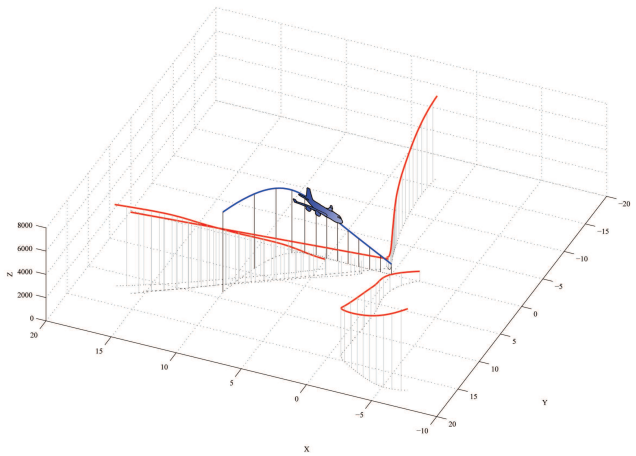

Figure 11. Own track of an aircraft (with symbol). The tracks of previous aircraft are also shown.

The aircraft receives a wind profile from the ground station at the same rate as observations from the other aircraft come in. Hence, the Kalman gain is fairly constant for this altitude as it receives data for this location exactly based on the wind profile received from ground. Once the data of the descending aircraft falls within the relevant altitude interval, the data is scaled with the C and R matrix and an additional term is included in the Kalman gain, increasing the value of Kalman gain for this altitude. Once the descending aircraft descends through 4,000 ft., the observations become irrelevant and the Kalman gain reverts back to the value based on the observations from the ground station.

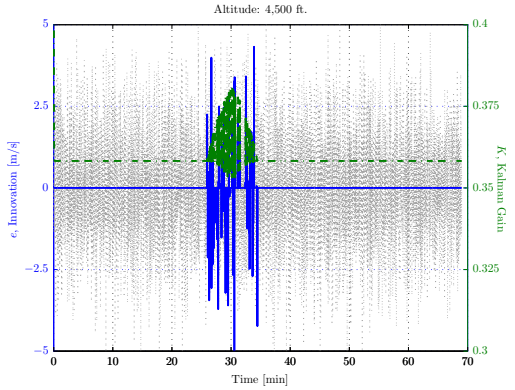

(a) Innovation step (solid line) due to descending aircraft, Innovation step from ground estimated profile (dotted line) and Kalman gain (dot-dashed line). Note that the observations from the other aircraft up to 25 minutes are disregarded because they are taken above the altitude of interest for our own aircraft.

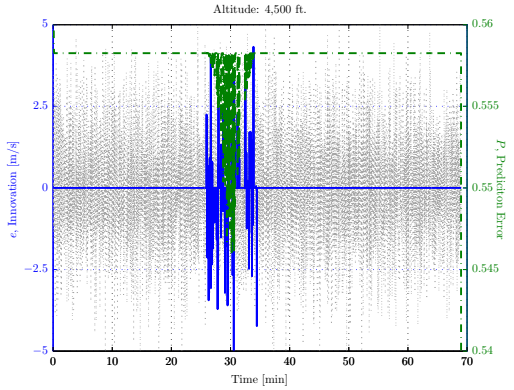

(b) Development of the Error covariance matrix P in time. The black crosses indicate that a new measurement has come in at that time. Note that the observations up to 23 minutes are disregarded because they are taken above the altitude of interest.

Figure 12. Performance metrics of the Wind Estimator.

According to Kalman filter theory, the accuracy of an estimate depends on the quality of the system model, the accuracy of the available measurements and the amount of measurements. In this case, the system dynamics are zero, so the accuracy of the wind estimation depends on the measurements solely. Therefore, it is hypothesized that the Kalman filter prediction error will decrease as more data becomes available.

Section 12(b) shows that while time goes by without (significant) measurements coming in (so up to 25 minutes), the value of P remains constant, but decreases as soon as observations from the other aircraft come in. This lower covariance means the uncertainty about the quality of the current estimate decreases. As a consequence,

- when a new single measurement comes in, it will be assigned a relatively high weight; the confidence in the current estimated value has dropped with respect to the confidence in the new measured value, and
- when new data becomes available the uncertainty in the estimate is reduced. This can be seen in the decrease of P whenever a measurement comes in, starting at $T = 25$ minutes.

IV.B. Performance accuracy

In order to see how well the noise is filtered from the observation data, an extra noise has been added to the data set. So for this case, an available observation set is considered to be the true wind speed, which is to be estimated. A normally distributed noise (mean: 0, std: 1.5 m/s (3 kts, representing the average FMS noise)) is added to this data set, to represent the incoming measurements. These simulated measurements are the input for the AWEA algorithm. The estimate it produces can then be compared to the real values. This process is shown in Fig. 13(a). The 'true' values (taken from the observation data) are represented by the circles, while their noisy counterparts are depicted as crosses. The estimate is shown in the solid line.

To check the robustness of the simulation, a bootstrap sample has been used to calculate the mean and standard deviation of the Root Mean Squared (RMS) of the prediction error. For this case, the RMS of the prediction error is around 0.67 m/s, see Fig. 13(b). For comparison, the RMS of the (simulated) measurement deviation is depicted on the right in the same figure.

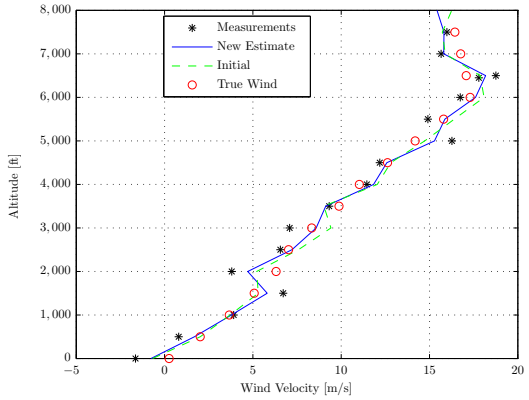

(a) Wind profile estimate with simulated observations.

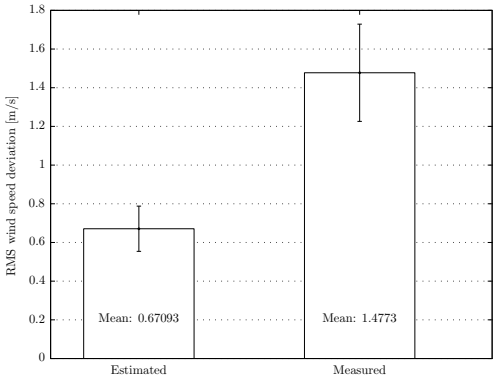

(b) RMS of the wind speed prediction error.

Figure 13. Accuracy of the Wind Estimator for simulated observations.

V. Conclusion

The proposed algorithms estimates wind profiles based on the meteorological data broadcast by nearby aircraft and/or other sources, effectively using them as real-time wind sensors in the TMA. The algorithm has the advantage of producing high-fidelity, high-resolution wind profiles that can immediately be used. Advanced approach procedures that require constant trajectory prediction and optimization can directly utilize the produced profiles. Validating the algorithm against a set of AMDAR data from Chicago O'Hare showed that the RMS of the prediction error is in the order of 0.67 m/s which is of a lower order than the accuracy of the observed measurements.

References

[1]Klooster, J. K., Wickman, K. D., and Bleeker, O. F., "4D Trajectory and Time-of-Arrival Control to Enable Continuous Descent Arrivals," *Proceedings of the AIAA Guidance, Navigation and Control Conference and Exhibit, Honolulu, Hawaii, 18 - 21 August*, No. AIAA 2008-7402, 2008, pp. 1–17.

[2]Coppenbarger, R. A., Mead, R. W., and Sweet, D. N., "Field Evaluation of the Tailored Arrivals Concept for Datalink-Enabled Continuous Descent Approach," *Journal of Aircraft*, Vol. 46, No. 4, 2009, pp. 1200–1209.

[3]De Prins, J. L., Schippers, K. F. M., Mulder, M., Van Paassen, M. M., In 't Veld, A. C., and Clarke, J.-P. B., "Enhanced Self-Spacing Algorithm for Three-Degree Decelerating Approaches," *Journal of Guidance, Control and Dynamics*, Vol. 30, No. 2, 2007, pp. 576–590.

[4]De Gaay Fortman, W. F., Van Paassen, M. M., Mulder, M., In 't Veld, A. C., and Clarke, J.-P. B., "Implementing Time-Based Spacing for Decelerating Approaches," *Journal of Aircraft*, Vol. 44, No. 1, 2007, pp. 106–118.

[5]De Leege, A. M. P., In 't Veld, A. C., Mulder, M., and Van Paassen, M. M., "Three-Degree Decelerating Approaches in Arrival Streams," *Proceedings of the AIAA Guidance, Navigation and Control Conference and Exhibit, Honolulu, Hawaii, 18 - 21 August*, No. AIAA 2008-7403, 2008, pp. 1–25.

[6]AMDAR Panel, "Aircraft Meteorological Data Relay (AMDAR) Reference Manual," Tech. rep., World Meteorological Organization, 2003.

[7]Moninger, W. R., Mamrosh, R. D., and Pauley, P. M., "Automated Meteorological Reports from Commercial Aircraft," Technical Report ARP 5430, World Meteorological Society, 2003.

[8]Delahaye, D., Puechmorel, S., and Vacher, P., "Windfield estimation by radar track Kalman filtering and vector spline extrapolation," *22nd Digital Avionics Systems Conference, 2003. DASC '03*, Vol. 1, October 2003, pp. 5.E.2 – 51–11.

[9]Mondoloni, S., "A Multiple-Scale Model of Wind-Prediction Uncertainty and Application to Trajectory Prediction," *Proceedings of the 6th AIAA Aviation Technology, Integration, and Operations Conference (ATIO), Wichita, KA, September 25-27*, No. AIAA 2006-7807, 2006, pp. 1 – 14.

[10]Wieringa, J. and Rijkoort, P., *Windklimmaat van Nederland*, Staatsuitgeverij, Den Haag, 1983, (in Dutch).

[11]Steentjes, A. P. W., *Design and development of a generic terrain-based wind atmosphere module for future flight simulators*, MSc Thesis, Faculty of Aerospace Engineering, Delft University of Technology, 2001.

[12]Wieringa, J., *De atmosferische grenslaag*, Lecture notes, Faculty of Applied Sciences, Delft University of Technology, 1987, (in Dutch).

[13]Hewitt, C. N. and Jackson, A. V., *Handbook of atmospheric science, principles and applications*, Blackwell, 2003.

[14]Baarspul, M., *Flight simulation techniques*, Faculty of Aerospace Engineering, Delft University of Technology, Delft, The Netherlands, 1982.

[15]Zoumakis, N. M. and Kelessis, A. G., "Methodology for Bulk Approximation of the Wind Profile Power-Law Exponent under Stable Stratification," *Boundary-Layer Meteorology*, Vol. 55, No. 1-2, 1990, pp. 199–203.

[16]SESAR, "The ATM Deployment Sequence," Deliverable 4, EUROCONTROL, January 2008.

[17]SESAR, "SESAR Master Plan D5," Deliverable 5, EUROCONTROL, April 2008.

[18]NextGen Office, "FAA's NextGen Implementation Plan 2010," Tech. rep., FAA, 800 Independence Avenue, Washington, DC, March 2010.